Nano Energy 67 (2020) 104268

Contents lists available at ScienceDirect

Nano Energy

journal homepage: http://www.elsevier.com/locate/nanoen

Full paper

Gating-induced reversible H_xVO_2 phase transformations for neuromorphic computing

Chen Ge [a,b,*,1], Ge Li [a,c,1], Qing-li Zhou [c], Jian-yu Du [a], Er-jia Guo [a,d], Meng He [a], Can Wang [a,b,e], Guo-zhen Yang [a], Kui-juan Jin [a,b,e,**]

[a] Beijing National Laboratory for Condensed Matter Physics, Institute of Physics, Chinese Academy of Sciences, Beijing, 100190, China
[b] School of Physical Sciences, University of Chinese Academy of Science, Beijing, 100049, China
[c] Key Laboratory of Terahertz Optoelectronics, Ministry of Education, Beijing Advanced Innovation Center for Imaging Theory and Technology, Department of Physics, Capital Normal University, Beijing, 100048, China
[d] Center of Materials Science and Optoelectronics Engineering, University of Chinese Academy of Sciences, Beijing, 100049, China
[e] Songshan Lake Materials Laboratory, Dongguan, 523808, China

ARTICLE INFO

Keywords:
Synaptic transistor
Electrolyte gating
VO_2
Artificial synapse
Phase transformation

ABSTRACT

Neuromorphic networks that consist of electronic synapses are very important for energy-efficient artificial intelligent applications. Therefore, in recent years, many efforts have been made to design and improve artificial synaptic devices to effectively mimic brain-spiking activity in biological synapses. In this work, we demonstrate a novel synaptic transistor based on the VO_2 film that uses the electrolyte gating at room temperature. Through the gating-induced protonation and deprotonation, we realize reversible phase transformations between various H-doped phases, which is confirmed by many characterization measurements. The VO_2 synaptic transistor based on the exploiting nonvolatile multi-level conductance states with various hydrogen doping concentrations can successfully emulate essential synaptic functions such as synaptic plasticity and spiking-time-dependent plasticity. An artificial neural network containing the VO_2 synaptic transistors simulated with supervised learning shows high recognition accuracy for the MNIST handwritten recognition dataset. This study provides a promising approach to develop high-performance electronic synaptic transistors by utilizing advanced Mott materials.

1. Introduction

Recently, tremendous efforts have been devoted to realizing an artificial brain-like computer, also known as the neuromorphic computation, which is vital for energy-efficient artificial intelligent applications [1–4]. A key step towards this goal is to construct high-performance electronic devices capable of accurately emulating the synaptic plasticity of biological synapses [5–11]. To that end, the nonvolatile conductance states of the designed electronic synaptic devices should be modulated continuously to mimic synaptic functions [7,12]. It is highly desirable to harness the material systems in which a nonvolatile multilevel resistance switching, and an electrically controllable metal-insulator transition (MIT) are present simultaneously [13]. Vanadium dioxide (VO_2), an archetypal Mott material, has the potential to become the material foundation of neuromorphic circuits. Besides, because its MIT occurs at about 341 K, which is slightly above room temperature, VO_2 has been extensively studied [14]. During the phase transition, VO_2 undergoes a reversible resistance change between the high-temperature metallic tetragonal phase and the low-temperature insulating monoclinic phase [15]. The temperature-driven change in the electrical resistance can reach several orders of magnitude, and the major variation of the electrical resistance happens around the phase transition temperature [16]. The intrinsic MIT feature makes VO_2 a promising candidate material for designing novel electronic synapses.

Protonation of VO_2 (H_xVO_2) is a feasible method to reduce its MIT temperature and manipulate the electronic states without destroying its lattice framework. Moreover, several recent works proved that protons (H^+), the smallest functional ions, can be injected into and released from VO_2 using the catalytic spillover method via the thermal annealing under H_2/vacuum conditions [17,18]. Also, the doped hydrogen in VO_2

* Corresponding author. Beijing National Laboratory for Condensed Matter Physics, Institute of Physics, Chinese Academy of Sciences, Beijing, 100190, China.
** Corresponding author. Beijing National Laboratory for Condensed Matter Physics, Institute of Physics, Chinese Academy of Sciences, Beijing, 100190, China.
E-mail addresses: gechen@iphy.ac.cn (C. Ge), kjjin@iphy.ac.cn (K.-j. Jin).
[1] These authors contributed equally.

https://doi.org/10.1016/j.nanoen.2019.104268
Received 3 October 2019; Received in revised form 31 October 2019; Accepted 4 November 2019
Available online 6 November 2019

can supply electrons, leading to the band-filling-controlled phase transformations, depending on the proton doping concentration [19]. However, the VO_2 protonation via a high-temperature heat treatment limits its application in neuromorphic electronic devices. Recently, the electrolyte gating has emerged as an intriguing method to manipulate phase transformations of transition metal oxide films electrically by doping functional ions at the room temperature [20]. Several works demonstrated the reversible modulation of the MIT in VO_2 films by electrolyte gating induced protonation/deprotonation processes [19,21–24]. Recently, electrolyte-gated synaptic transistors have attracted much attention because of their potential high-performance [25,26]. Shi et al. reported an electrolyte-gated transistor with $SmNiO_3$, which realized a synaptic spike-timing-dependent plasticity learning behavior [27]. Zhu et al. reported an oxide-based artificial synapse network coupled by proton neurotransmitters [10]. Yang et al. emulated the ionic modulation process of biological synapses, and controlled the transition from short-term to long-term memory using different gate voltage amplitude in an electrolyte-gated WO_3 transistor [8]. He et al. proposed the multiterminal oxide-based transistor for spatiotemporal information processing by mimicking the dendritic discriminability of different spatiotemporal input sequences [28]. These experimental results have inspired the exploring of synaptic transistors based on the electrolyte-gated VO_2 films.

In this study, the reversible phase transformations in VO_2 epitaxial films are achieved by inserting and extracting hydrogen via electrolyte gating at the room temperature, as presented in Fig. 1a. The evolution of crystal and electronic structures during the electrolyte gating is systematically investigated. Then, a novel synaptic transistor is developed by harnessing the nonvolatile multi-level conductance states depending on various hydrogen doping concentrations. A VO_2 synaptic transistor exhibits essential functions such as synaptic plasticity and spiking-time-dependent plasticity. Simulations of an artificial neural network consisting of the VO_2 synaptic transistors showed that the proposed system could achieve high classification accuracy. Due to the MIT nature of VO_2, the presented electrolyte-gated synaptic transistor provides a unique opportunity to realize hardware implementation of high-performance artificial neural networks.

2. Results and discussion

We grew epitaxial the VO_2 films with the MIT at about 341 K (Fig. 1b) on (0001) Al_2O_3 substrates by using the pulsed laser deposition (PLD) technique (refer to Methods Section for details). The X-ray diffraction (XRD) patterns indicated that only VO_2 $(020)_M$ family peaks emerged without other vanadium oxide phases (Fig. S1). Then, we verified the phase transformations in VO_2 thin films under electrolyte gating. A liquid electrolyte, N,N-diethyl-N-(2-methoxyethyl)-N-methylammonium bis-(trifluoromethylsulphonyl)-imide (DEME-TFSI), was adopted as a gating medium [29]. We would like to point out that solid electrolytes are more appealing for practical devices from a technological point of view. Positive (negative) gating voltages induced the intercalation (extraction) of hydrogen ions into (from) the VO_2 thin films. The electrolyte-gating driven protonation led to the formation of stable H_xVO_2 phases. First, the protonation process in our VO_2 films after positive gating was confirmed by performing the secondary ion mass spectrometry (SIMS) measurements. The doped hydrogen concentration increased with the positive gating (Fig. S2). The hydrogen required during the gating-induced phase transformation could come from the water content of ionic liquids [30,31] confirmed by the SIMS depth profile of D^+ ions in the gated VO_2 films with the ionic liquids containing heavy water D_2O (Fig. S2). The evolution of electronic phase transformations in H_xVO_2 was investigated based on the temperature

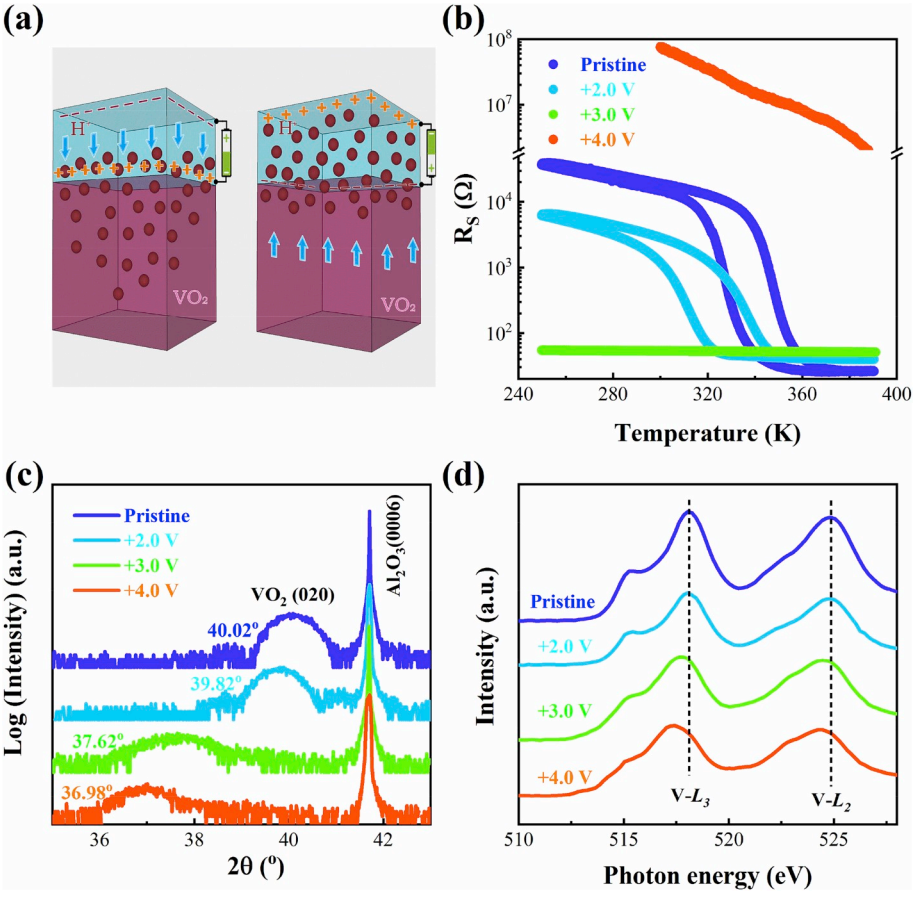

Fig. 1. Electrolyte gating induced phase transformations. (a) The schematic diagram of hydrogen ion movement during the electrolyte gating. (b) Temperature-dependent sheet resistance in VO_2 films at various gate voltages varying from 0 to +4.0 V. (c) The X-ray diffraction (XRD) patterns near Al_2O_3 (0006) peak of the VO_2 epitaxial films after applying various gate voltages varying from 0 to +4.0 V. (d) The X-ray absorption spectra (XAS) of V *L*-edge of the VO_2 films at various gate voltages varying from 0 to +4.0 V. The gating time at +2.0 V, +3.0 V, and +4.0 V is 30 min, 60 min, and 120 min, respectively.

dependence of the sheet resistance (R_S) with varying gating voltage and time (Fig. 1b). The pristine VO_2 film showed a typical temperature-dependent MIT, in which R_S decreased by three orders of magnitude at about 341 K. By doping the hydrogen into the VO_2 films during the electrolyte gating, the value of R_S in the low-temperature insulating phase gradually decreased, and the metallic H_xVO_2 phase emerged. Interestingly, further hydrogenation induced a dramatic phase transition from the metallic H_xVO_2 to other insulating HVO_2 states. Thus, tristate phase transformations between the insulating VO_2, metallic H_xVO_2, and insulating HVO_2 could be achieved depending on the doped hydrogen amount in the electrolyte gating.

We measured the XRD θ–2θ scans of the VO_2 films after various positive gating to explore the structural phase transformations during the electrolyte gating (Fig. 1c). The XRD peak of the $(020)_M$ diffraction of the pristine VO_2 film shifted towards a small angle with the increase in the doped hydrogen content, and the peak eventually reached 36.98° in the insulating HVO_2 phase. The shift of the XRD peak is ascribed to the intercalation of hydrogen ions into the thin films. To clarify the phenomena of hydrogen doping via electrolyte gating, we characterized the electronic structures of the insulating VO_2, metallic H_xVO_2, and insulating HVO_2 using the synchrotron-based X-ray absorption spectroscopy (XAS) of the V-*L* edge (Fig. 1d). The V-L_3 edge exhibited a peak shift to the lower energy direction upon the protonation, reflecting that the V atoms transformed towards a lower valence state [31]. Associated with the evolution of electronic structures, the optical transparency of the thin film could be electrically switched by doping the hydrogen (Fig. S3). The pristine VO_2 and metallic H_xVO_2 films showed a deep yellow color, while the HVO_2 film was almost transparent in the range from visible to the infrared band (Fig. S3). All the mentioned physical properties make the electrolyte-gated VO_2 thin films highly promising material for application in robust synaptic transistors.

We designed an electrolyte-gated transistor with the co-planar gate electrodes using the VO_2 epitaxial films as a channel material to emulate the biological synapses. The schematic diagram of the device structure is illustrated in Fig. 2a. More details about the device fabrication can be found in Methods Section. The current-voltage (*I*–*V*) curve between the source and drain electrodes exhibited a good ohmic contact (Fig. S4). The gating-induced tristate phase transformation of the VO_2 channel was also demonstrated by measuring the conductance (G) as a function of time under various positive V_G (Fig. 2b). It can be seen that G slightly increased under the gate voltage lower than the threshold value (~1.23 V) of the hydrolysis reaction. Under the medium gate voltage ($1.23\ V < V_G < 2.0\ V$) G monotonically increased, indicating the phase transformation from the insulating VO_2 to the metallic H_xVO_2. With the application of high V_G ($V_G > 2.0$ V), G of the channel first increased, and then gradually decreased. This process implied that the tristate phase transformations happened from the insulating VO_2 to the metallic H_xVO_2, and then to the insulating HVO_2. Thus, it can be concluded that both the gating voltage and gating time are important for the hydrogen intercalation into the VO_2 lattice. The doped hydrogen concentration determines the phase transformations. Here, we applied medium V_G ($1.23\ V < V_G < 2.0\ V$) to avoid the second phase transformation from H_xVO_2 to HVO_2. The unique tristate phase transformations in VO_2 could be applied where a single voltage is required to realize both potentiation and depression.

The transfer curve was measured by sweeping V_G from 0 to 2.0 V, then from 2.0 V to −1.5 V, and finally, from −1.5 V back to 0 (Fig. 2c). The source-drain voltage V_{SD} was kept constant at 50 mV, and the sweeping rate was 0.5 mV/s. The transfer curve exhibited a clear hysteresis loop. The source-drain current (I_{SD}) gradually increased from 20 nA to 2300 nA as V_G increased from 0 to 2.0 V. The high conductance state was maintained at $V_G = 0$, implying its non-volatility. Under negative gating, the high conductance state could be reversed to its pristine low conductance state. The gate leakage current I_G was at least two orders of magnitude smaller than I_{SD}, indicating that I_G had a negligible effect on device performance (Fig. 2c). Therefore, the channel conductance G could be effectively adjusted between low and high conductance states by controlling the insertion and extraction of H^+ into the VO_2 channel.

Reversible phase transformations between the insulating VO_2 and the metallic H_xVO_2 were further confirmed by adjusting V_G as a function of gating time (Fig. 2d). The channel conductance G was monitored over time by switching the polarity of constant V_G. Under a constant V_G of +1.5 V, G gradually increased from 0.22 μS to 9.85 μS, due to the protonation process induced by positive electrolyte gating. Once V_G was switched to - 1.0 V, G decreased to 0.23 μS, due to the deprotonation

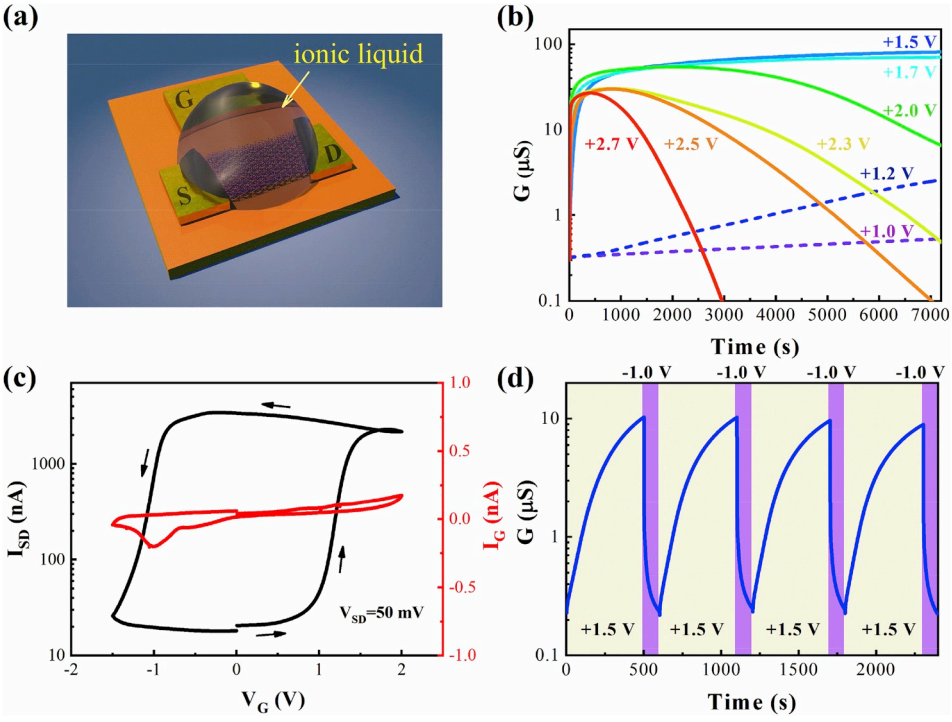

Fig. 2. Electrolyte-gated VO_2 transistor. (a) The schematic illustration of the transistor structure. The VO_2 films form the channel between the source (S) and drain (D) electrodes, and an ionic liquid (DEME-TFSI) is used as a gating medium. (b) Measured channel conductance G of a 10-nm thick VO_2 film as a function of time at various gate biases from +1.0 V to +2.7 V. (c) The transfer curve at $-1.5\ V \le V_G \le 2.0$ V. The red curve denotes the gate leakage current during the transfer curve measurement. The gate voltage V_G was swept with a speed of 0.5 mV/s. The arrows show the direction of the gate bias sweep. (d) Reversible phase transformations between the insulating VO_2 and the metallic H_xVO_2 by applying alternating positive (+1.5 V) and negative (−1.0 V) V_G as a function of gating time. A constant source-drain voltage $V_{SD} = 50$ mV was applied to monitor the channel conductance.

process induced by negative electrolyte gating. Thus, the reversible protonation and deprotonation phase transformations could be manipulated by applying alternating positive and negative V_G in the electrolyte-gated VO_2 transistor (Fig. 2d).

The external pulses were applied to the gate electrodes to control the hydrogen insertion and extraction in the VO_2 channel, which could emulate various synaptic functions in biological synapses. We applied the gate pulses to trigger the change in the amplitude of I_{SD}, similar to the excitatory postsynaptic currents (EPSCs) under presynaptic spikes. The pulse width was fixed at 200 ms, and the channel current was monitored at a small V_{SD} of 50 mV. The EPSCs increased with increasing the amplitude of V_G pulses. The EPSCs quickly decreased to the initial value under low V_G, while the EPSCs could not decrease to its initial value under high V_G exceeding the threshold value of the hydrolysis reaction (Fig. 3a). The electrostatic (low V_G) and electrochemical (high V_G) effects are responsible for the V_G-controlled transition from short-to long-term memory [8]. As it is well known, in biological synapses, successive external stimuli can lead to an increase in the number of neurotransmitters from the presynaptic membrane to the synaptic cleft. Similarly, successive electrical pulses can effectively modulate the EPSCs by increasing the doped H^+ concentration in artificial synapses (Fig. 3b). Therefore, the pulse width was fixed at 200 ms, and the pulse voltage V_G was +1.5 V. The EPSCs could be increased by increasing the pulse width of the presynaptic spikes (Fig. S5). The multi-level states required for synaptic functions were demonstrated in the electrolyte-gated VO_2 transistor by sending a series of V_G pulses to the gate electrode (Fig. S6). Various H-doped VO_2 phases could keep stable during at least 3500 s, demonstrating their good retention property (Fig. S7). The calculated energy consumptions per spike (4.2 fJ, short-term memory; 2.2 pJ, long-term memory) were several orders of magnitude lower than that (~900 pJ) of the artificial synapses based on conventional CMOS circuits [32] (Fig. S8). Although the energy

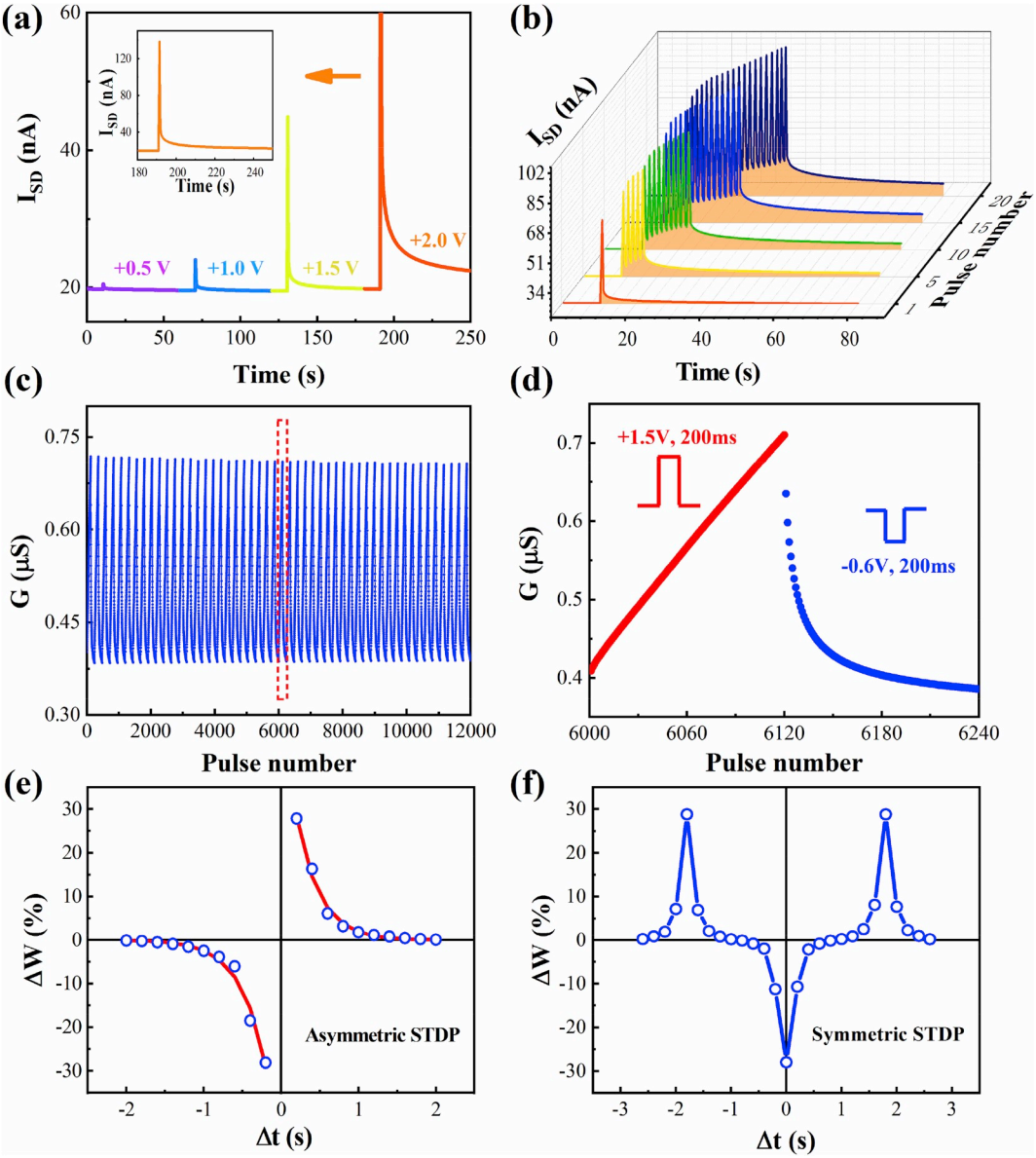

Fig. 3. The VO_2 synaptic transistor characteristics for neuromorphic computing. (a) The EPSCs induced by a series of V_G pulses with the same pulse width of 200 ms and different amplitudes, +0.5 V, +1.0 V, +1.5 V, and +2.0 V. The inset shows the full spike triggered by a +2.0 V pulse. (b) The EPSCs stimulated by a series of V_G pulses (1, 5, 10, 15, 20 spikes) with the same amplitude of voltage (+1.5 V). (c) The V_G-controlled long-term potentiation and depression processes for 120 positive (+1.5 V for 200 ms, spaced 600 ms apart) and 120 negative (−0.6 V for 200 ms, spaced 600 ms apart) V_G pulses. There are 50 cycles for LTP and LTD. (d) The zoom-in view shows a cycle for gating-induced LTP and LTD processes. Asymmetric (e) and symmetric (f) STDP function implemented in the ferrite synaptic transistor. Δt denotes the difference between the pre and post-neuron spikes. A constant source-drain voltage $V_{SD} = 50$ mV was applied to monitor the channel conductance.

consumption per spike for the long-term memory in our electrolyte-gated VO_2 transistor was still higher than that of biological synapses (1–10 fJ), it could be comparable to those of the electrolyte-gated synaptic transistors in recent reports [4]. These results verify that the electrolyte-gated VO_2 transistor can potentially emulate the synaptic plasticity that is essential for biological synapses to perform signal processing and neural computation.

We further mimicked the long-term synaptic plasticity, including the long-term potentiation (LTP) and long-term depression (LTD) in our synaptic transistor (Fig. 3c). The LTP and LTD denoted persistent increase and decrease in synaptic strength at a certain number of external stimuli, respectively. The long-term synaptic plasticity is an essential design requirement for brain-like computing [33]. The multi-level nonvolatile states can be realized with a number of consecutive V_G pulses to tune G by doping protons into the VO_2 channel. The amount of H^+ ions intercalated in VO_2 is precisely manipulated by V_G pulses, and this process is reversible. Therefore, to emulate the LTP, we applied 120 positive V_G pulses (the amplitude of +1.5 V, the pulse duration of 200 ms). The channel conduction G increased during the gradual phase transformation from the insulating VO_2 to the metallic H_xVO_2. In contrast, the LTD appeared when 120 negative V_G pulses (−0.6 V, 200 ms) were applied to the gate electrode. Negative gating tends to extract H^+ ions from the channel, leading to a transformation from the metallic H_xVO_2 phase to the insulating VO_2 phase. Thus, successive negative gate spikes can decrease the EPSC. Here, G was measured at V_{SD} of 50 mV. The potentiation and depression of synaptic weight could be mimicked by applying consecutive positive and negative spikes, reflecting reproducible switching (Fig. 3c). Fig. 3d shows a single cycle of G modulation for the LTP and LTD processes. Obviously, the LTP exhibited high linearity. For the LTD, in the beginning, G of the device varied greatly with the voltage pulses sent to the gate terminal. The change in G of the device decreased gradually with a continuous voltage pulse. Therefore, further investigations are required to improve the linearity during the LTD process in future.

In neurobiology, memory is associated with the strength of a synaptic connection, which is called synaptic weight. The spike-timing-dependent plasticity (STDP) plays an important part in information processing and brain network functions [34,35]. The STDP is regarded as one of the essential Hebbian learning rules, which indicates the modification of a synaptic weight induced by a relative timing of correlated spikes between the connected neurons. The sign and magnitude of a change in a synaptic weight depends on Δt, which is defined as a relative time interval of the pre- and post-synaptic spikes. For an asymmetric STDP, the LTP occurs when a post-synaptic spike is fired before a pre-synaptic spike ($\Delta t < 0$), while the LTD occurs when a pre-synaptic spike is applied before a post-synaptic spike ($\Delta t > 0$). A significant change in the synaptic plasticity occurs at a short Δt, whereas a small change in the synaptic plasticity happens at a long Δt. We successfully demonstrated the asymmetric STDP functions in the electrolyte-gated VO_2 synaptic transistor (Fig. 3e). A multiplexer was connected to the gate electrode of the device to convert the time difference between pre- and post-synaptic spikes [36]. For more details about the circuitry, refer to Fig. S9 in the Supplementary Material. The measured asymmetric STDP curve could be fitted with an exponentially decaying function and emulate the behavior of a biological synaptic system [34]. We also realized the symmetric STDP function by changing the shape of the source spike (Fig. 3f). For the symmetric STDP, the percent change in the channel conductance only depends on the absolute value of Δt. The successful STDP implementation in the electrolyte-gated VO_2 synaptic transistor indicates a potential application of Mott materials in neuromorphic device development.

We further evaluated the performance of the artificial neural network consisting of the electrolyte-gated VO_2 synaptic transistors using the experimentally measured LTP and LTD states (Fig. 3c). This artificial neural network was trained with two data sets, 8×8 pixels images (small images) of handwritten digits from the University of California at Irvine (UCI) image dataset [37], and 28×28 pixels images (large images) of handwritten digits from the Modified National Institute of Standards and Technology (MNIST) handwritten dataset [38], by using the back-propagation algorithm. We utilized a simple three-layer network structure with only one hidden layer to implement the simulation using Cross Sim simulator (Fig. 4a). A crossbar, regarded as a part of a "neural core", was employed to perform vector-matrix multiplication and outer-product update operations (Fig. 4b) [39,40]. The cumulative distribution functions during the potentiation and depression processes are plotted in Fig. S10 of the Supplementary Material. It can be seen that the linearity during the potentiation (protonation) was better than during the depression (deprotonation). The artificial neural network consisting of the electrolyte-gated VO_2 synaptic transistors achieved high classification accuracy (Fig. 4c and d). The results of the training were comparable to the ideal performance of the floating-point-based neural network, which represents the theoretical limit for the simulator. In identifying the small digits, the classification accuracy reached 91% in the second training epoch and approached 94% after 20 training epochs (Fig. 4c). In identifying the large digits, the simulation results showed that the artificial neural network with VO_2 synaptic transistors could reach the classification accuracy of 91% (Fig. 4d). The obtained classification accuracy was slightly lower than that reported in the related recent works about synaptic devices [39,40]. It should be noted that the obtained classification accuracy was higher than that obtained with two-terminal resistive and phase-change memory devices (20%–82%) [41–45]. However, to realize a higher recognition accuracy and improve the device performance in this VO_2 synaptic transistor, further works are still required to improve the linearity and symmetry during the potentiation and depression processes.

3. Conclusion

In summary, a novel electrolyte-gated synaptic transistor based on a typical Mott material VO_2 is designed. We realized the reversible phase transformations via gating-controlled protonation and deprotonation in VO_2 films. It is shown that by finely tuning the hydrogen doping concentration, the electrolyte-gated VO_2 transistor exhibits multi-level nonvolatile conductance states, which is required for artificial synapses. Besides, the VO_2 electronic synapses with a three-terminal configuration can successfully emulate important synaptic functions such as synaptic plasticity and spiking-time-dependent plasticity. An artificial neural network consisting of VO_2 synaptic transistors trained with supervised learning achieved high recognition accuracy of 91% for the MNIST handwritten recognition dataset. Our findings provide a new design direction of electrolyte-gated synaptic transistors based on advanced Mott electronic materials.

4. Methods

4.1. Sample preparation

The VO_2 thin films with a thickness of 10 nm were epitaxially grown on (0001) Al_2O_3 substrates (MTI Ltd.) using the pulsed laser deposition with a 308-nm XeCl excimer laser, an energy density of about 0.2 J/cm^2, and a repletion rate of 2 Hz. The VO_2 films were deposited at 375 °C in a flowing oxygen atmosphere at the oxygen pressure of 1.0 Pa, and cooled down to the room temperature at the cooling speed of 20 °C/min. The deposition rate of VO_2 films was calibrated by X-ray Reflection (XRR).

4.2. Device fabrication

The thin films were patterned into channels with a coplanar gate structure using standard photolithography and argon-ion etching. The channel size is 50 μm × 210 μm. The length between the gate electrode and channel is 50 μm. The Cr/Au (2 nm/70 nm) layer was prepared as

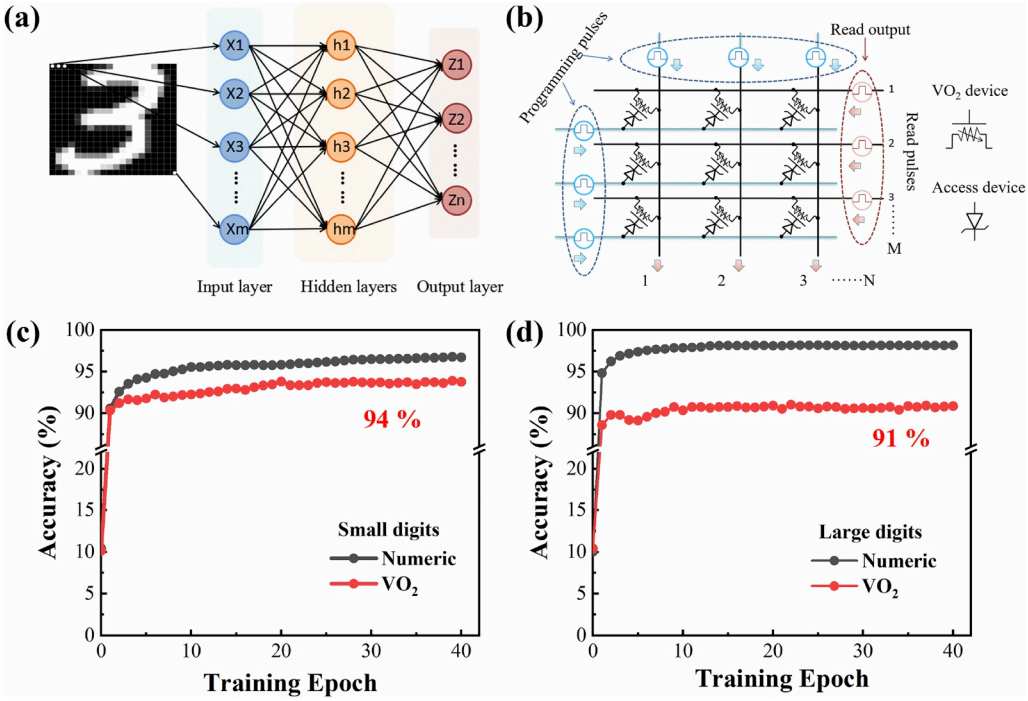

Fig. 4. Image recognition simulations with VO_2 synaptic transistors. (a) Schematic of a three-layer neural network with one hidden layer. (b) Schematic of a neural core with a synaptic layer composed of an electrolyte-gated VO_2 transistor crossbar array and access devices. Classification accuracy change with the number of training epochs for (c) small digits and (d) large digits with an ideal device and a VO_2 synaptic transistor.

electrodes via thermal evaporation. An overlayer of a hard-baked photoresist was used as an isolation layer to prevent electric leakage between gate and source electrodes. The transistor device was completed by dropping an ionic liquid N, N-diethyl-N-(2-methoxyethyl)-N-methylammoniumbis-(trifluoromethylsulphonyl)-imide (DEME-TFSI) on the channel and gate electrodes.

4.3. Sample characterization

X-ray diffraction (XRD) measurements were performed using a Rigaku SmartLab instrument. Optical transmittance spectra were taken in air at room temperature with spectrophotometers (Cary 5000 UV–Vis–NIR, Agilent and Excalibur 3100, Varian). The thickness of VO_2 films on double polished Al_2O_3 substrates for transmittance spectra measurements is 50 nm. XAS measurements were performed via total electron yield method, and the background vacuum level was 6×10^{-7} Torr.

4.4. Electrical measurement

The electrical characteristics of the electrolyte-gated VO_2 devices were measured in a Lakeshore probe station with a Keithley 4200 semiconductor parameter analyser at ambient conditions. The sweeping rate was 0.5 mV/s for the transfer curve. We applied V_G at room temperature, and then measured temperature-dependent R_S. The measurements for temperature-dependent R_S were done with a 2400 Sourcemeter and a Keithley 2182 Nanovoltmeter in PPMS (Quantum Design Ltd.).

Declaration of competing interest

The authors declare that they have no known competing financial interests or personal relationships that could have appeared to influence the work reported in this paper.

Acknowledgments

This work was supported by National Key R&D Program of China (No. 2017YFA0303604), the National Natural Science Foundation of China (Nos. 11674385, 11404380, 11721404, 11874412, and 11574219), the Youth Innovation Promotion Association of CAS (No. 2018008), and the Key Research Program of Frontier Sciences CAS (No. QYZDJSSW-SLH020). The authors would like to thank 4B9B beamline of the Beijing Synchrotron Radiation Facility (BSRF) and BL12B beamline in National Synchrotron Radiation Laboratory.

Appendix A. Supplementary data

Supplementary data to this article can be found online at https://doi.org/10.1016/j.nanoen.2019.104268.

References

[1] Y. LeCun, Y. Bengio, G. Hinton, Nature 521 (2015) 436.
[2] M.A. Zidan, J.P. Strachan, W.D. Lu, Nat. Electron. 1 (2018) 22.
[3] Y. van de Burgt, A. Melianas, S.T. Keene, G. Malliaras, A. Salleo, Nat. Electron. 1 (2018) 386.
[4] C. Ge, C.X. Liu, Q.L. Zhou, Q.H. Zhang, J.Y. Du, J.K. Li, C. Wang, L. Gu, G.Z. Yang, K.J. Jin, Adv. Mater. 31 (2019) 1900379.
[5] J. Rivnay, S. Inal, A. Salleo, R.M. Owens, M. Berggren, G.G. Malliaras, Nat. Rev. Mater. 3 (2018) 17086.
[6] S.Y. Zhao, Z.Y. Ni, H. Tan, Y. Wang, H. Jin, T.X. Nie, M.S. Xu, X.D. Pi, D.R. Yang, Nano Energy 54 (2018) 383.
[7] S.M. Yu, Proc. IEEE 106 (2018) 260.
[8] J.T. Yang, C. Ge, J.Y. Du, H.Y. Huang, M. He, C. Wang, H.B. Lu, G.Z. Yang, K.J. Jin, Adv. Mater. 30 (2018) 1801548.
[9] J. Zhu, Y. Yang, R. Jia, Z. Liang, W. Zhu, Z.U. Rehman, L. Bao, X. Zhang, Y. Cai, L. Song, R. Huang, Adv. Mater. 30 (2018) 1800195.
[10] L.Q. Zhu, C.J. Wan, L.Q. Guo, Y. Shi, Q. Wan, Nat. Commun. 5 (2014) 3158.
[11] L. Yin, C. Han, Q.T. Zhang, Z.Y. Ni, S.Y. Zhao, K. Wang, D.S. Li, M.S. Xu, H.Q. Wu, X.D. Pi, D.R. Yang, Nano Energy 63 (2019) 103859.
[12] Q.Z. Wan, M.T. Sharbati, J.R. Erickson, Y.H. Du, F. Xiong, Adv. Mater. Technol. 4 (2019) 1900037.
[13] Y. Zhou, S. Ramanathan, Proc. IEEE 103 (2015) 1289.

[14] N.B. Aetukuri, A.X. Gray, M. Drouard, M. Cossale, L. Gao, A.H. Reid, R. Kukreja, H. Ohldag, C.A. Jenkins, E. Arenholz, K.P. Roche, H.A. Durr, M.G. Samant, S.S. P. Parkin, Nat. Phys. 9 (2013) 661.
[15] D. Lee, B. Chung, Y. Shi, G.Y. Kim, N. Campbell, F. Xue, K. Song, S.Y. Choi, J. P. Podkaminer, T.H. Kim, P.J. Ryan, J.W. Kim, T.R. Paudel, J.H. Kang, J. W. Spinuzzi, D.A. Tenne, E.Y. Tsymbal, M.S. Rzchowski, L.Q. Chen, J. Lee, C. B. Eom, Science 362 (2018) 1037.
[16] Y.L. Chen, Z.W. Wang, S. Chen, H. Ren, B.W. Li, W.S. Yan, G.B. Zhang, J. Jiang, C. W. Zou, Nano Energy 51 (2018) 300.
[17] J. Wei, H. Ji, W.H. Guo, A.H. Nevidomskyy, D. Natelson, Nat. Nanotechnol. 7 (2012) 357.
[18] H. Yoon, M. Choi, T.W. Lim, H. Kwon, K. Ihm, J.K. Kim, S.Y. Choi, J. Son, Nat. Mater. 15 (2016) 1113.
[19] T. Katase, K. Endo, T. Tohei, Y. Ikuhara, H. Ohta, Adv. Electron. Mater. 1 (2015) 1500063.
[20] C. Leighton, Nat. Mater. 18 (2019) 13.
[21] S. Chen, Z.W. Wang, H. Ren, Y.L. Chen, W.S. Yan, C.M. Wang, B.W. Li, J. Jiang, C. W. Zou, Sci. Adv. 5 (2019), eaav6815.
[22] M. Jo, H.J. Lee, C. Oh, H. Yoon, J.Y. Jo, J. Son, Adv. Funct. Mater. 28 (2018) 1802003.
[23] K. Shibuya, A. Sawa, Adv. Electron. Mater. 2 (2016) 1500131.
[24] H. Ji, J. Wei, D. Natelson, Nano Lett. 12 (2012) 2988.
[25] H. Han, H.Y. Yu, H.H. Wei, J.D. Gong, W.T. Xu, Small 15 (2019) 1900695.
[26] S.L. Dai, Y.W. Zhao, Y. Wang, J.Y. Zhang, L. Fang, S. Jin, Y.L. Shao, J. Huang, Adv. Funct. Mater. 29 (2019) 1903700.
[27] J. Shi, S.D. Ha, Y. Zhou, F. Schoofs, S. Ramanathan, Nat. Commun. 4 (2013) 2672.
[28] Y.L. He, S. Nie, R. Liu, S.S. Jiang, Y. Shi, Q. Wan, Adv. Mater. 31 (2019) 1900903.
[29] C. Ge, K.J. Jin, L. Gu, L.C. Peng, Y.S. Hu, H.Z. Guo, H.F. Shi, J.K. Li, J.O. Wang, X. X. Guo, C. Wang, M. He, H.B. Lu, G.Z. Yang, Adv. Mater. Interfaces 2 (2015) 1500407.
[30] N. Lu, P. Zhang, Q. Zhang, R. Qiao, Q. He, H.-B. Li, Y. Wang, J. Guo, D. Zhang, Z. Duan, Z.L. Li, M. Wang, S.Z. Yang, M.Z. Yan, E. Arenholz, S.Y. Zhou, W.L. Yang, L. Gu, C.W. Nan, J. Wu, Y. Tokura, P. Yu, Nature 546 (2017) 124.
[31] R. Zimmermann, R. Claessen, F. Reinert, P. Steiner, S. Hüfner, J. Phys. Condens. Matter 10 (1998) 5697.
[32] E. Chicca, D. Badoni, V. Dante, M. D'Andreagiovanni, G. Salina, L. Carota, S. Fusi, P. Del Giudice, IEEE Trans. Neural Netw. 14 (2003) 1297.
[33] R.A. John, N. Yantara, Y.F. Ng, G. Narasimman, E. Mosconi, D. Meggiolaro, M. R. Kulkarni, P.K. Gopalakrishnan, C.A. Nguyen, F. De Angelis, S.G. Mhaisalkar, A. Basu, N. Mathews, Adv. Mater. 30 (2018) 1805454.
[34] G.Q. Bi, M.M. Poo, Annu. Rev. Neurosci. 24 (2001) 139.
[35] J.M. Young, W.J. Waleszczyk, C. Wang, M.B. Calford, B. Dreher, K. Obermayer, Nat. Neurosci. 10 (2007) 887.
[36] Y. Nishitani, Y. Kaneko, M. Ueda, T. Morie, E. Fujii, J. Appl. Phys. 111 (2012) 124108.
[37] K. Bache, M. Lichman, UCI Machine Learning Repository, University of California at Irvine, School of Information and Computer Science, Irvine, CA, USA, 2016.
[38] Y. Lecun, C. Cortes, C.J. Burges, The MNIST Database of Handwritten Digits, National Institute of Standards and Technology, Gaithersburg, MD, USA, 2016.
[39] Y. van de Burgt, E. Lubberman, E.J. Fuller, S.T. Keene, G.C. Faria, S. Agarwal, M. J. Marinella, A.A. Talin, A. Salleo, Nat. Mater. 16 (2017) 414.
[40] E. Fuller, F. Gabaly, F. Léonard, S. Agarwal, S. Plimpton, R. Jacobs-Gedrim, C. James, M. Marinella, A. Talin, Adv. Mater. 29 (2017) 1604310.
[41] S. Park, A. Sheri, J. Kim, J. Noh, J. Jang, M. Jeon, B. Lee, B. Lee, H.J. Hwang, in: Proc. IEEE Int. Electron Devices Meeting, IEEE, Washington, DC, USA, 2013, p. 854.
[42] I.T. Wang, Y.C. Lin, Y.F. Wang, C.W. Hsu, T.H. Hou, in: Proc. IEEE Int. Electron Devices Meeting, IEEE, San Francisco, CA, USA, 2014, p. 665.
[43] G.W. Burr, R.M. Shelby, S. Sidler, C. Nolfo, J. Jang, I. Boybat, R.S. Shenoy, P. Narayanan, K. Virwani, E.U. Giacometti, B.N. Kurdi, H. Hwang, IEEE Trans. Electron Devices 62 (2015) 3498.
[44] P.Y. Chen, B. Lin, I.T. Wang, T.H. Hou, J. Ye, S. Vrudhula, J.S. Seo, Y. Cao, S. Yu, in: IEEE/ACM Int. Conf. On Computer-Aided Design (ICCAD), IEEE, Austin, TX, USA, 2015, p. 194.
[45] R.B. Jacobs-Gedrim, S. Agarwal, K.E. Knisely, J.E. Stevens, M.S. von Heukelom, D. R. Hughart, J. Niroula, C.D. James, M.J. Marinella, in: IEEE Int. Conf. On Rebooting Computing (ICRC), IEEE, Washington, DC, USA, 2017, p. 1.

Chen Ge is currently an associate professor at the Institute of Physics, Chinese Academy of Sciences. He received Ph.D degree from Institute of Physics, Chinese Academy of Sciences in 2012. His research interests include emerging memory and artificial synapse devices based on oxide epitaxial films.

Ge Li received her BS degree in 2017 from the Department of Physics, Capital Normal University, Beijing, China. She is currently a Master student in the Department of Physics, Capital Normal University, and has joint training in the Institute of Physics, Chinese Academy of Sciences. Her research interests include electrolyte gated synaptic transistors and THz metamaterials.

Qingli Zhou received her PhD degree from the Institute of Physics, Chinese Academy of Sciences, Beijing, China, in 2006. She is currently an Associate Professor studied in terahertz spectroscopy in the Department of Physics, Capital Normal University, Beijing, China. Her research interests focus on THz metamaterials and their applications in biosensing, dynamical THz modulator.

Jianyu Du received his Master's degree in 2017 from China University of Geosciences, Beijing, China. He is currently a doctoral candidate in the Institute of Physics, Chinese Academy of Sciences, Beijing, China. His research focuses on designing high-performance artificial synapses.

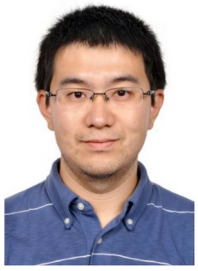

Prof. Er-Jia Guo received his Ph. D degree from Institute of Physics (IOP), Chinese Academy of Sciences (CAS). He joined IOP-CAS in 2018 after the postdoc. at Leibniz Institute of Solid State Materials (IFW), University of Mainz, and Oak Ridge National Laboratory. His research interest is the transition metal oxide thin films and heterostructures.

Meng He is currently an engineer in Institute of Physics, Chinese Academy of Sciences. Her research interest focus on oxide epitaxial thin films.

Prof. Can Wang received his Ph. D degree in physics from the Institute of Solid State Physics, Chinese Academy of Sciences. He is a Professor at the Institute of Physics, Chinese Academy of Sciences. His research focuses on epitaxial oxide thin films and heterostructures.

Prof. Guozhen Yang is a professor at the Institute of Physics, Chinese Academy of Sciences. He was elected as an academician of the Chinese Academy of Sciences in 1999. His research interests focus on optics and condensed matter physics.

Prof. Kui-juan Jin received her Ph. D. degree and became a professor at the Institute of Physics, Chinese Academy of Sciences in 1995 and 2004, respectively. She is a Fellow of the Institute of Physics of UK and a Fellow of the American Physical Society. Her main research is in the crossing area of optics and low dimensional perovskite oxides.